Check for updates

AGU ADVANCING EARTH AND SPACE SCIENCE

Geophysical Research Letters

RESEARCH LETTER
10.1029/2021GL093094

Key Points:

- Two sprite events featured with halo were captured on the high-speed video camera with coordinated broadband sferic data
- In both cases, the halo initiated within 0.5 ms after the causative return stroke
- The induction component of lightning-induced transient *E*-field appears to make a considerable contribution to the halo formation

Correspondence to:

G. Lu,
gaopenglu@gmail.com

Citation:

Ren, H., Lu, G., Cummer, S. A., Peng, K.-M., Lyons, W. A., Liu, F., et al. (2021). Comparison between high-speed video observation of sprites and broadband sferic measurements. *Geophysical Research Letters*, *48*, e2021GL093094. https://doi.org/10.1029/2021GL093094

Received 22 FEB 2021
Accepted 14 APR 2021

© 2021. American Geophysical Union. All Rights Reserved.

Comparison Between High-Speed Video Observation of Sprites and Broadband Sferic Measurements

Huan Ren[1], Gaopeng Lu[1,2,3], Steven A. Cummer[4], Kang-Ming Peng[1], Walter A. Lyons[5], Feifan Liu[1], Xiao Li[6,7], Yongping Wang[1], Shoubao Zhang[8], and Zhengwei Cheng[9]

[1]School of Earth and Space Sciences, University of Science and Technology of China, Hefei, Anhui, China, [2]Key Laboratory of Atmospheric Optics, Anhui Institute of Optics and Fine Mechanics, HFIPS, Chinese Academy of Sciences, Hefei, Anhui, China, [3]Collaborative Innovation Center on Forecast and Evaluation of Meteorological Disasters, Nanjing University of Information Science & Technology, Nanjing, Jiangsu, China, [4]Electrical and Computer Engineering Department, Duke University, Durham, NC, USA, [5]FMA Research, Fort Collins, CO, USA, [6]University of Chinese Academy of Sciences, Beijing, China, [7]Key Laboratory for Middle Atmosphere and Global Environment Observation (LAGEO), Institute of Atmospheric Physics, Chinese Academy of Sciences, Beijing, China, [8]China Research Institute of Radiowave Propagation, Qingdao, Shandong, China, [9]State Key Laboratory of Space Weather, National Space Science Center, Chinese Academy of Sciences, Beijing, China

Abstract High-speed video observations of two sprites with halo features were analyzed with concurrent measurements of broadband magnetic sferics. Both events were produced by positive cloud-to-ground (CG) strokes. Moreover, the halo features appeared less than 0.5 ms after the return stroke, and the first sprite elements followed within 1 and 3 ms, respectively, for the two cases. The persistent charge transfer in the causative stroke from long continuing current can maintain the continuous glowing of existing sprite elements, and also may aid the vertical development and enhanced luminescence of later sprite elements. The observations with electric field (*E*-field) simulations by the transmission line model provide evidence that the induction component of the lightning-induced *E*-field contributes significantly to halo formation. Our results suggest additional measurements and analysis are needed to identify the specific role of induction *E*-field in addition to the well-known quasi-electrostatic (QE) field in the lightning-induced impact on the mesosphere.

Plain Language Summary We analyze two cases of sprite observations demonstrating the halo feature that were both produced by positive cloud-to-ground (CG) strokes over a mesoscale convective system in the central United States. The first event was the brightest sprites observed on that night, while the second event was a dancing sprite event containing three sprite elements all following a single +CG. The broadband (<1 Hz–400 kHz) lightning sferic signals recorded at various ranges are analyzed in comparison with the high-speed and low-light-level video to reveal the detailed development and evolution of sprite events. The first case contains an elves, halo, and sprite elements; the second case includes a halo as well as three sprite elements. In both case, the halo features appeared less than 0.5 ms after the return stroke. From this observation with relatively high time resolution and the simulation of lightning-induced electrical field (*E*-field) change at the height of halo formation, we attribute the occurrence of halo to the induction *E*-field from the initial portion (within 1 ms) of charge transfer in the causative stroke mainly. The continuous illumination of the existing sprite element and the time delay and vertical structure of following sprites are associated with the subsequent continuing current of causative strokes.

1. Introduction

Transient Luminous Events (TLEs) are caused by the coupling of electromagnetic energy released by tropospheric lightning into the middle atmosphere (Pasko et al., 1998). As a major category of TLEs, red sprites are readily recorded in both ground-based and space-born observations with high-sensitivity optical devices (Boccippio et al., 1995; Franz et al., 1990; Lu et al., 2017; Lyons, 1996). Sprites generally occur in the altitude range of 40–90 km above energetic thunderstorms (Sentman et al., 1995; Winckler, 1995), and those observed over continental thunderstorms are predominantly (>99%) produced by positive cloud-to-ground

(CG) strokes (Cummer & Lyons, 2005; Huang et al., 1999; Li et al., 2012). At present, the charge moment change (CMC) caused by parent lightning is understood to be critical metric to evaluate the potential of sprite production (Pasko, Inan, Bell, & Taranenko, 1997). According to existing studies, the CMC required for producing a sprite is found to be as low as +120 C km (Hu et al., 2002). Huang et al. (1999) analyzed many sprite-producing CG strokes generated by one thunderstorm and found a minimum CMC of +300 C km for sprite production. Models including the quasi-electrostatic (QE) field theory (Hiraki & Fukunishi, 2006; Pasko, Inan, Bell, & Taranenko, 1997; Qin et al., 2011), full-wave electromagnetic field model (De Larquier & Pasko, 2010; Li et al., 2012), as well as the transmission line (TL) method (Lu, 2006; Ren et al., 2019) have been proposed to simulate the electric field (*E*-field) perturbation caused by CG strokes at high altitudes. By separating the *E*-field into three components as static, induction, and radiation components, Ren et al. (2019) suggested that the inductive *E*-field excited by the causative stroke might play a significant role in the sprite initiation.

For TLE observations, high-speed video has been an effective tool. It can not only provide the time-resolved evolution in the fine structure of sprites (Stanley et al., 1999), but also provide the high time resolution to compare the dynamic sprite evolution with the time-resolved charge transfer through the synchronized sferic measurements (Cummer & Stanley, 1999; Li et al., 2008). High-speed imaging has also been applied to examine the dynamic development and optical characteristics of sprites with halo feature (Cummer et al., 2006). However, sprite events with halo features have yet to be analyzed on sub-millisecond time scales in comparison with concurrent measurement of causative charge transfer.

In this paper, we analyze the high-speed video observations of two sprites that both demonstrate halo features over a mesoscale convective system (MCS) in central United States. Low-frequency (LF, 25 kHz–400 kHz) magnetic signals sampled at 1 MHz are applied for the first time to provide a higher time resolution to determine the onset of causative return strokes. Our study demonstrates a higher time resolution in the high-speed video observation and magnetic signal measurement than previous studies, which is of great significance for studying the formation mechanism of halo and sprite features. In addition, we calculated the *E*-field components at the moment of halo initiation with the TL model, and our results confirmed that the inductive *E*-field excited by the causative stroke might play a significant role in the halo formation.

2. Observations and Measurement

On the night of June 12, 2013, a total of 51 sprites were recorded over an MCS in the central United States by an intensified high-speed camera, a low-light-level video camera (SpriteCam), and several radio-frequency magnetic sensors. Two sprites with halo features were selected to examine in detail because of the relatively high quality of combined data acquisition. The parent strokes of both events were located by the National Lightning Location Network (NLDN) with peak current of +197 and +117 kA, respectively. Figure 1 shows the location of these two events. The first one (Event A) was generated by the first return stroke of a positive CG flash at 0627:43 UTC (+45.0777°N, −102.0647°E), which was the brightest sprite observed on that day. The second sprite was a dancing event (Event B) containing three sprite elements generated by a positive CG stroke at 0742:59 UTC (+44.9542°N, −99.7575°E).

The reflectivity echo from the NEXRAD weather radar located in Rapid City, South Dakota is shown in Figure 1. Both events were observed over the stratiform region, and the second was relatively close to the convective zone. The observation sites are shown in Figure 1. The sprites were observed simultaneously on the SpriteCam at Bennett, Colorado (+39.693°N, −104.488°E), a high-speed camera at Yucca Ridge Field Station (YR; +40.702°N, −105.030°E) near Fort Collins, Colorado, LF sferic measurement on the campus of Oklahoma University (+35.975°N, −79.100°E), and VLF/ULF sferic measurements in Duke Forest (+35.182°N, −97.440°E) with low background noise level. All the measurements are synchronized by GPS with timing accuracy better than 1 μs.

SpriteCam captures TLEs in triggered mode (through the UFO Capture software). A video stream that spans over 2 s of a trigger event is saved at a standard NSTC rate of 30 frames per second (fps) (see Lu et al., 2013 for details). The intensified high-speed imaging system installed at Yucca Ridge Field Station is composed of a Vision Research Phantom 7.1 monochrome high-speed camera and an ITT Gen III image intensifier with the spectral response in the range of 450–900 nm. The image size of the high-speed camera is 800 × 600

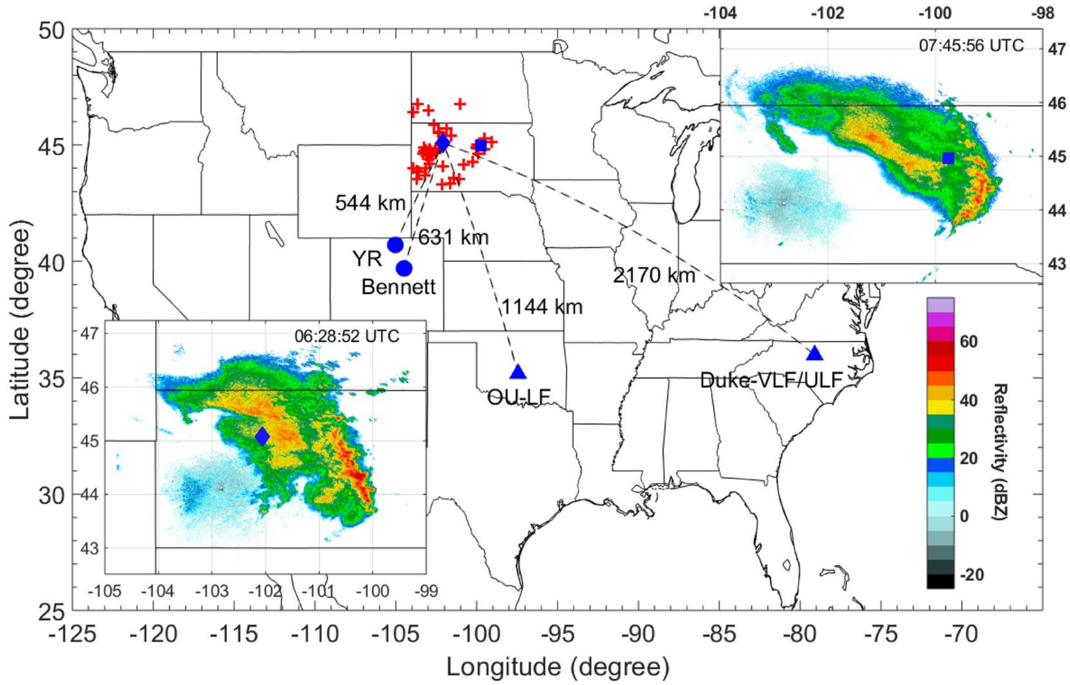

Figure 1. Observation configuration and radar reflectivity field (dBZ). The four observation instrumentations include a SpriteCam at Bennett, Colorado (blue circle), an intensified high-speed camera at Yucca Ridge Field Station (YR; blue circle) near Fort Collins, Colorado, radio frequency magnetic sensors near Duke University (blue triangle), and Oklahoma University (OU; blue triangle). The geolocation of parent lightning of Event A is marked by the blue diamond, while Event B is marked by the blue square. All the parent lightning of sprites that are detected by NLDN on the same day are labeled by the red crosses. NLDN, National Lightning Location Network.

pixels and the frame rate is set to 8,000 and 10,000 fps, respectively, for the two sprites examined here. Various magnetic sensors are coordinated to record lightning signals over a wide frequency range (<1 Hz–300 kHz) from ultralow frequency (ULF, <1 Hz –400 Hz, sampling at 2,500 Hz), very-low frequency (VLF, 50 Hz–30 kHz, sampled at 100 kHz) to low frequency (LF, 30–300 kHz, sampled at 1 MHz). The LF sferic signal of sprite-producing positive CG (SP + CG) strokes usually appears as a burst of impulsive signals over microseconds and can be used for accurately determining the onset of return stroke.

3. Analysis and Results

In this section, we examine the detailed halo and sprite evolution in Events A and B. In both events, the occurrence of halo preceded the sprite; as also indicated by the observations of Stenbaek-Nielsen et al. (2013) and Cummer et al. (2006), some sprites appear to initiate from the bottom of halo region. The luminosity curves of two events are acquired based on the high-speed imaging results and the city background light is removed (the area confined by the red rectangle in Figures 2 and 3 defines the region of luminosity calculation). We also deduce the time-resolved current moment and CMC waveform along a vertical lightning channel from the VLF and ULF data with the deconvolution method of Cummer and Inan (2000). The height of sprites is estimated according to the following process: we correct the azimuth and elevation angle of each pixel in low-light-level images through the star field; then, the height of sprites is estimated by placing the sprites right above the causative stroke located by the NLDN and using the elevation angle. The halos in both events are centered at about 80 km (e.g., Wescott et al., 2001), which is assumed to be the occurrence height of two events. Then, the luminosity curve of both events and the LF, VLF, ULF signals, and CMC for two SP + CGs are subtracted with the propagation delay relative to the source point (namely all the measurements are time-aligned at the source and the curvature of the Earth is considered). Since the analyses are focused on the temporal relationship between sprites and causative lightning strokes, the amplitude of all the waveforms is normalized with the peak.

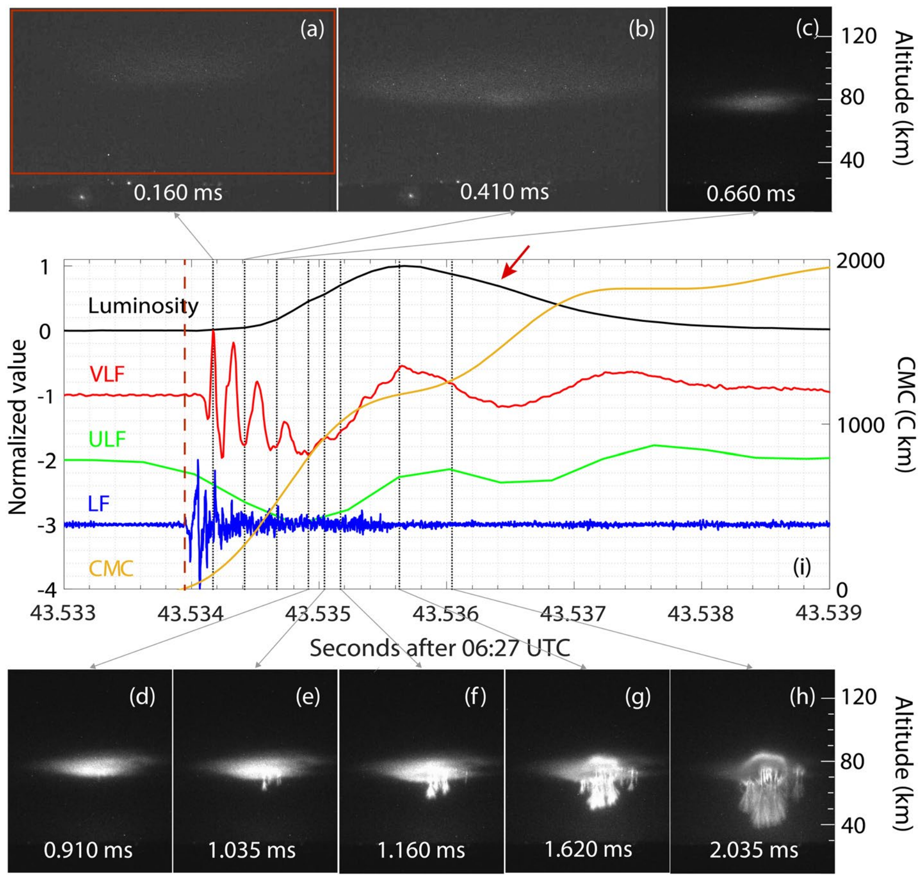

Figure 2. (a)–(h) The contrast-enhanced high-speed images of Event A at 0627:43 UTC; (i) The high-speed luminosity variation, the RF signal waveforms and CMC waveform of Event A at 0627:43 UTC, the vertical dashed line indicates the onset of the return stroke.

3.1. Event A at 0627:43 UTC

The high-speed images of Event A are shown in Figures 2a–2h. As the luminous area is not bright enough and it is difficult to be recognized by naked eyes, we enhance the contrast of images. From Figures 2a and 2b, we can see a light-emitting area with a gradually increasing spatial scale from the top (about 95 km) to bottom (about 85 km) within 0.25 ms. The altitude and timescale of elves are typically confined in the altitude range of 85–95 km (Barrington-Leigh & Inan, 1999; Marshall, 2012) and less than 0.5 ms (Newsome & Inan, 2010). Yue and Lyons (2015) also examined an elves event with the modulation of gravity wave at 0359:13 UTC on the same night. The elves in our case was generated about 0.16 ms after the onset of return stroke (inferred from the LF magnetic signal and indicated in Figure 2i with a red vertical dashed line). Since elves is attributed to the electromagnetic perturbations at the bottom of ionosphere after an intense CG stroke (Nagano et al., 2003; Rowland, 1998; Taranenko et al., 1993), it should start almost at the same time with the return stroke, which cannot be further distinguished with the temporal resolution (about 0.125 ms) of our high-speed video. Moreover, it takes about 5.9 μs for the average radiative lifetime of N_2 (B) between the excitation of elves by the electromagnetic pulse and the light emission of elves (Morrill et al., 1998). Such factors could cause the time difference between the appearance of elves and return stroke in this case.

The halo began to appear at 0.41 ms after the return stroke when the CMC accumulated to about +300 C km, by starting to glow from the bottom center of the elves that descent vertically and expanded laterally (Figure 2b). Lu (2006) calculated the static, induction and radiation components in the elves region based on the TL model, and suggested that the induction term plays a significant role in a small region (with radius *r* of about 11 km) at an altitude of 90 km above the stroke. Their simulation results are generally consistent with

10.1029/2021GL093094

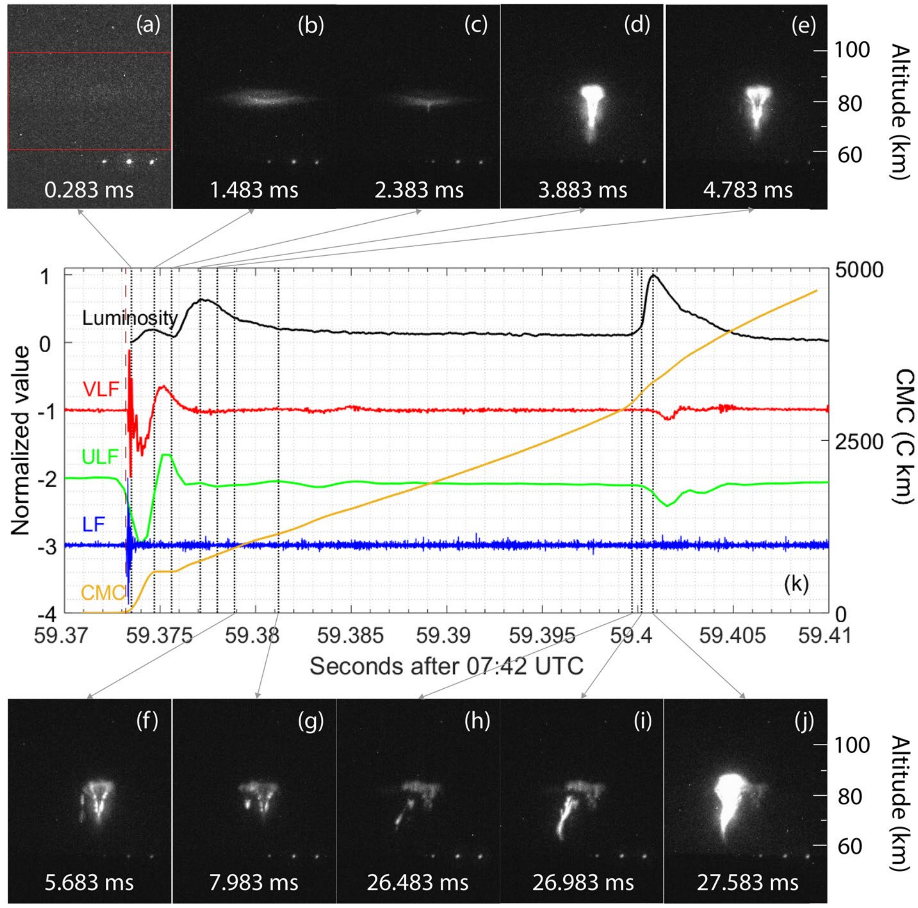

Figure 3. (a)–(j) Contrast-enhanced high-speed images of Event B at 0742:59 UTC; (k) high-speed luminosity variation, the RF signal and CMC waveforms of Event B at 0742:59 UTC, the vertical dashed line indicates the onset of the return stroke.

the observations of this event. The halo reached its maximum brightness before the sprite began to appear at the center of its bottom (Figure 2d). The evolution from its generation to a full development almost occurred before the ULF signal reaches the first peak. In other words, the halo occurred before the maximum charge transfer of the causative CG. Recently, Ren et al. (2019) calculated the individual components in the halo region based on the TL model. It is inferred that before the static component dominants, the induction term with amplitude more than half of the total *E*-field directly above the lightning might play a critical role in the halo formation. This case corroborates the result of Ren et al. (2019) with the observational fact that the halo could be attributed to the induction term driven by the impulsive charge transfer.

The sprite appeared when the CMC accumulated to about +900 C km (Figure 2d) at about 0.91 ms after the return stroke, and reached the greatest brightness (Figure 2g) approximately 0.5 ms later. As time elapses, the contribution of the static term at the altitude of 80 km gradually increases until it becomes completely dominated (Ren et al., 2019). The CMC of Event A reached about +1200 C km when the sprite reached its brightest state. The initial part (<1 ms) of continuing current is the main contributor of halo production; meanwhile, the sprite following the halo is caused by the subsequent long-lasting continuing current, as also shown by Li et al. (2008). We can also see the maximum brightness is almost in line with the signature of sprite current, which is consistent with Cummer et al. (1998). The small time difference could be attributed to that as the halo and sprite are intertwined in the same event, the obtained luminosity curve was an overlapped effect; therefore, it does not merely reflect the evolution of sprite. As we can see from the figure, during the occurrence of sprite current, a slight bump (red arrow in Figure 2) in the luminosity curve is barely discernible, which could be caused by the peak brightness of sprite.

3.2. Event B at 0742:59 UTC

For Event B as a dancing sprite event at 0742:59 UTC, as shown in Figure 3a, the halo appeared when the CMC accumulated to about +250 C km at approximately 0.28 ms after the onset of the return stroke (inferred from the LF magnetic signal as indicated in Figure 3k with a red vertical dashed line), and it reached the peak luminosity (Figure 3b) roughly 1.2 ms later by centering at an altitude of about 80 km. The high local electron density and the fast electrical relaxation lead to the appearance of halo instead of sprite streamers.

The first sprite element initiated from the center bottom of the halo (Figure 3c) about 2.38 ms after the return stroke upon a cumulative CMC of +625 C km. Then, it reached its peak brightness 1.5 ms later. The second sprite element initiated (Figure 3e) in the lower-left area of the first one before the first one faded away. Thus, we cannot clearly distinguish the inception of the second element from its luminosity variation. However, according to the images from the high-speed video, the second sprite element initiated at about 4.78 ms after the return stroke.

The third sprite element initiated (Figure 3h) in the lower-left area of the second one at about 26.5 ms after the return stroke, when the CMC has accumulated to +3125 C km. The time delay of sprite occurrence relative to the causative return stroke varies broadly from <1 ms to more than 200 ms; most of them were within 20 ms after the return stroke (Hu et al., 2002; Li et al., 2008). Therefore, this was a very long delayed sprite element. Event B maintained certain brightness before the third sprite element initiated (Figures 3g and 3h) during the continuing current. The third sprite element had the longest delay and also the highest brightness (Figure 3j). The continuing current might have kept building up the high-altitude *E*-field and maintained the intense *E*-field region for the following sprite. The impulse current (Bell et al., 1998; Cummer & Lyons, 2005; Gomes & Cooray, 1998) or continuous current lasting several tens of milliseconds can transfer a large amount of charge from cloud to ground (Cummer & Füllekrug, 2001). The rapid charge transfer from thundercloud generates a transient *E*-field at the mesospheric altitude (Pasko, Inan, Bell, & Taranenko, 1997), which may exceed the threshold of conventional dielectric breakdown and trigger the streamer development to form sprites (Liu & Pasko, 2004; Pasko et al., 1998; Qin et al., 2011). For the occurrence of sprites, the long-term maintenance of a transient *E*-field at high altitude may be even more important than the peak strength of *E*-field (Pasko et al., 1999). In this case, the continuous charge transfer maintained a high *E*-field in the region where the sprite was generated. Meanwhile, we can see that the corresponding VLF perturbation appeared during the occurrence of the third sprite element. Both successive intense CG strokes and a single stroke with a series of current surges superposed on an intense continuing current could produce dancing sprites (Lu et al., 2013). Therefore, a relatively small magnetic disturbance could also excite a bright sprite element. In addition, Qin et al. (2011) suggested that the triggering of long-delayed sprites might be a unique property of halos produced by positive CG strokes due to the formation of a long-lasting high *E*-field region. The continuing current further enlarges this high *E*-field region and reduces the sprite altitude to a region with a smaller electron density, which could cause a long-time delay and vertical structure for some sprites. In comparison with Event A, Event B endured 10 times longer although the total CMC was approximately twice that of the former. Although both the intensity and time scale of the continuing current are important to the initiation of sprite, the time scale appears to contribute more to the persistence of sprite brightness, and the total CMC is more important for the brightness. More sprites events should be analyzed to reveal the details regarding this statement.

4. Discussions and Conclusions

The lightning-induced *E*-field at halo and sprite altitudes can be calculated with the TL model to examine the contribution of individual components (e.g., Lu, 2006; Ren et al., 2019). The input current waveform is calculated from the time-resolved current moment as obtained in Section 3. As the halo is thought to appear directly above the vertical lightning channel (e.g., Wescott et al., 2001), and the radiation component is zero above the lightning channel, in the cylindrical coordinate system, the time-resolved vertical *E*-field (E_z) at location (φ, z, $r = 0$) can be calculated as:

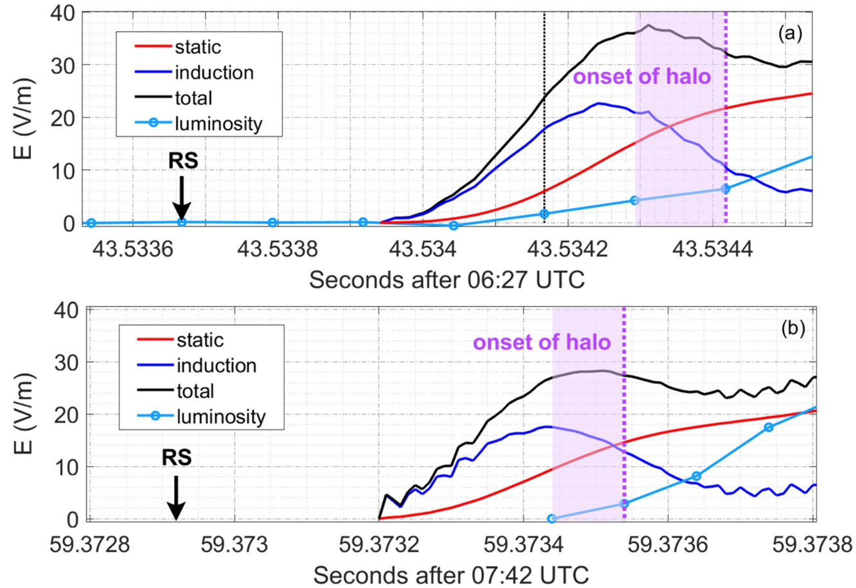

Figure 4. (a) Lightning induced *E*-field at halo initiation altitude of Event A at 0627:43 UTC; (b) lightning induced *E*-field at halo initiation altitude of Event B at 0742:59 UTC. The hollow circle on the luminosity curve represents the value in the red box area of each high-speed camera image, the black arrows point to the onset of RS (return stroke).

$$E_z\left(\varphi,z,t\right)=\frac{1}{2\pi\varepsilon_0}\int_0^H\left[\frac{1}{\left(z-z'\right)^3}\int_0^t I\left(z',\tau-\frac{z'}{v}-\frac{z-z'}{c}\right)d\tau\right]dz'+\frac{1}{2\pi\varepsilon_0}\int_0^H\left[\frac{1}{c\left(z-z'\right)^2}I\left(z',t-\frac{z'}{v}-\frac{z-z'}{c}\right)\right]dz'$$

where H is the height of lightning channel; z' is the height of front edge of return stroke base current propagating in the lightning channel at time t; v is the constant return stroke speed; c is the speed of light in the air; dz' = 1 m is the length of the current element. All the *E*-field components are nearly vertical because the vertical *E*-field is dominant over the horizontal *E*-field within a small region above the lightning channel. The TL model clearly separates the static component generated from the charge displacement and the induction term generated by the movement of charge, but it does not reflect the influence due to the characteristics of high-altitude atmosphere. Compared to the Finite-Difference Time-Domain (FDTD) method incorporates the effects of ionization and absorption of the ionosphere (e.g., Zhang et al., 2014), it behaves almost the same as that of the FDTD method in the total *E*-field at 80 km altitude within 1 ms after the return stroke (Ren et al., 2019). Since we focus on the initiation of halo, the *E*-field within the previous phase is examined, as shown in Figure 4.

In addition to the time-resolved *E*-field components in the halo region centered at 80 km, the luminosity curves of both sprites examined are also shown in Figure 4. Before the halo appeared, the induction term remained higher than the static component, indicating that the induction term dominates the impact on the high-altitude mesosphere shortly after the return stroke. The purple dashed line represents the onset time of halo as captured by the high-speed camera, while due to the limited time resolution, it should be slightly behind the real onset, and the real halo onset should be in the shaded purple window. Therefore, the total *E*-field in the halo initiation area (shaded purple) for Event A (Figure 4a) and Event B (Figure 4b) is about 36 V/m and 28 V/m, respectively; in both cases, the induction component contributes roughly 50% to the total *E*-field upon the halo initiation. In addition, for Event A that contained an obvious elves feature, the onset of the elves indicated by the vertical black dashed line should be closer to the onset of *E*-field as the elves is mainly excited by the electromagnetic pulse (EMP) of return stroke, which means that in this case the contribution of induction component to the halo initiation is likely more significant.

The driving *E*-field of halo calculated in these two cases is somewhat lower than the vertical *E*-field threshold of dielectric breakdown (~48 V/m) calculated by Thomas et al. (2005) on the basis of the MSIS-E−90 atmosphere model. It is not surprising as there are many factors that could disturb the local condition (especially the neutral atmospheric density) at the altitude of halo initiation, such as gravity waves (Pasko, Inan, & Bell, 1997), chemical reactions, meteors in the mesosphere (Qin et al., 2014) and so on. As a matter of fact, Yue and Lyons (2015) reported the observation of elves at 0359:13 UTC on the same night, and the banded structure as observed by a collocated color near-infrared camera reflected the modulation of mesospheric state by the convectively generated gravity waves. Moreover, in addition to the two sprites examined, there were more than 50 sprites produced by the same thunderstorm, and it remains possible that the preceding lightning discharges could also disturb the local electrical parameters and make significant contributions to the initiation of subsequent sprites. Hu et al. (2007) applied the two-dimensional cylindrical full-wave FDTD model to simulate the lightning-generated electromagnetic waves at the mesospheric altitude by sprite-producing CG strokes, and the calculated electromagnetic field at the moment of sprite initiation was only 0.12–0.69 times the traditional breakdown threshold for nearly half cases they examined.

In summary, the coordinated observations of two sprites and their parent lightning on the night of June 12, 2013 over a mesoscale convective system were analyzed in this paper. The concurrent broadband (<1 Hz–400 kHz) lightning sferics are analyzed on the basis of high-speed imaging results to reveal the details regarding the temporal evolution of halo and sprite in comparison with the time-resolved charge transfer in the causative lightning stroke. In addition, the lightning-induced *E*-field perturbation at the altitude of halo initiation is calculated with the TL model to examine which component contributes the most to the halo initiation. The main conclusions are as follows:

1. When the return stroke starts, the halo appears almost immediately. In the first case, the elves, halo and sprite initiated at approximately 0.16, 0.41, and 0.91 ms after the return stroke. In the second case as a dancing sprite event, the halo and three sprite elements initiated at about 0.28, 2.38, 4.78, and 26.5 ms, respectively, after the return stroke. The initiation of red sprite is the combined effect of the driving *E*-field and the atmospheric background conditions at the initiation height, as well as their luminous duration. In the two cases, the different onset of halo and sprite elements suggests that the lightning *E*-field exceeded the threshold probably under varying mesospheric conditions. The sustaining luminosity of the halo and sprite suggests the state of the lightning *E*-field exceeding the threshold
2. The observed halos are mainly produced by the initial part (<1 ms) of the continuing current during the causative +CG stroke when the lightning current has reached the maximum while the resultant charge transfers barely started to cumulate; our analysis provides the observational evidence that in addition to the static component, the induction component also contributes to the formation of the halos, and its contribution actually dominates during the very initial stage. This means that for the initiation of halos, the *E*-field generated by the current pulse of charge transfer may be more important than that generated by the charge relocation
3. The subsequent continuing current of causative strokes seems to maintain the high *E*-field of sprite region and leads to a persistent illumination of the existing sprite. Moreover, it may contribute to the high luminosity and vertical structure of the sprite element followed when a smaller current surge appears

Data Availability Statement

The data examined in this paper are available at https://zenodo.org/record/3600940#.XhW4R3aATJ0.

Acknowledgments
This work was supported by National Key Research and Development Program of China (2017YFC1501501), National Natural Science Foundation of China (41622501, 41875006, 42005068 & U1938115), the Chinese Meridian Project, Fundamental Research Funds for the Central Universities (WK2080000134 & WK6030000114), and the US National Science Foundation Dynamic and Physical Meteorology program through grant AGS-2026304.

References

Barrington-Leigh, C. P., & Inan, U. S. (1999). Elves triggered by positive and negative lightning discharges. *Geophysical Research Letters*, *26*(6), 683–686. https://doi.org/10.1029/1999GL900059

Bell, T. F., Reising, S. C., & Inan, U. S. (1998). Intense continuing currents following positive cloud-to-ground lightning associated with red sprites. *Geophysical Research Letters*, *25*(8), 1285–1288. https://doi.org/10.1029/98GL00734

Boccippio, D. J., Williams, E. R., Heckman, S. J., Lyons, W. A., Baker, I. T., & Boldi, R. (1995). Sprites, ELF Transients, and Positive Ground Strokes. *Science*, *269*, 1088–1091. https://doi.org/10.1126/science.269.5227.1088

Cummer, S. A., & Füllekrug, M. (2001). Unusually intense continuing current in lightning produces delayed mesospheric breakdown. *Geophysical Research Letters*, *28*(3), 495–498. https://doi.org/10.1029/2000GL012214

Cummer, S. A., & Inan, U. S. (2000). Modeling ELF radio atmospheric propagation and extracting lightning currents from ELF observations. *Radio Science*, *35*(2), 385–394. https://doi.org/10.1029/1999RS002184

Cummer, S. A., Inan, U. S., Bell, T. F., & Barrington-Leigh, C. P. (1998). ELF radiation produced by electrical currents in sprites. *Geophysical Research Letters*, *25*(8), 1281–1284. https://doi.org/10.1029/98gl50937

Cummer, S. A., Jaugey, N., Li, J., Lyons, W. A., Nelson, T. E., & Gerken, E. A. (2006). Submillisecond imaging of sprite development and structure. *Geophysical Research Letters*, *33*(4), L04104. https://doi.org/10.1029/2005GL024969

Cummer, S. A., & Lyons, W. A. (2005). Implications of lightning charge moment changes for sprite initiation. *Journal of Geophysical Research*, *110*(A4), A04304. https://doi.org/10.1029/2004JA010812

Cummer, S. A., & Stanley, M. (1999). Submillisecond resolution lightning currents and sprite development: Observations and implications. *Geophysical Research Letters*, *26*(20), 3205–3208. https://doi.org/10.1029/1999GL003635

De Larquier, S., & Pasko, V. P. (2010). Mechanism of inverted-chirp infrasonic radiation from sprites. *Geophysical Research Letters*, *37*(24), L24803. https://doi.org/10.1029/2010GL045304

Franz, R. C., Nemzek, R. J., & Winckler, J. R. (1990). Television image of a large upward electrical discharge above a thunderstorm system. *Science*, *249*(4964), 48–51. https://doi.org/10.1126/science.249.4964.48

Gomes, C., & Cooray, V. (1998). Long impulse currents associated with positive return strokes. *Journal of Atmospheric and Solar-Terrestrial Physics*, *60*(7), 693–699. https://doi.org/10.1016/S1364-6826(98)00039-X

Hiraki, Y., & Fukunishi, H. (2006). Theoretical criterion of charge moment change by lightning for initiation of sprites. *Journal of Geophysical Research*, *111*(A11), A11305. https://doi.org/10.1029/2006JA011729

Huang, E., Williams, E., Boldi, R., Heckman, S., Lyons, W., Taylor, M., et al. (1999). Criteria for sprites and elves based on Schumann resonance observations. *Journal of Geophysical Research*, *104*(D14), 16943–16964. https://doi.org/10.1029/1999JD900139

Hu, W., Cummer, S. A., & Lyons, W. A. (2007). Testing sprite initiation theory using lightning measurements and modeled electromagnetic fields. *Journal of Geophysical Research*, *112*, D13115. https://doi.org/10.1029/2006JD007939

Hu, W., Cummer, S. A., Lyons, W. A., & Nelson, T. E. (2002). Lightning charge moment changes for the initiation of sprites. *Geophysical Research Letters*, *29*(8), 120. https://doi.org/10.1029/2001GL014593

Li, J., Cummer, S. A., Lyons, W. A., & Nelson, T. E. (2008). Coordinated analysis of delayed sprites with high-speed images and remote electromagnetic fields. *Journal of Geophysical Research*, *113*, D20206. https://doi.org/10.1029/2008JD010008

Li, J., Cummer, S., Lu, G., & Zigoneanu, L. (2012). Charge moment change and lightning-driven electric fields associated with negative sprites and halos. *Journal of Geophysical Research*, *117*, A09310. https://doi.org/10.1029/2012JA017731

Liu, N., & Pasko, V. P. (2004). Effects of photoionization on propagation and branching of positive and negative streamers in sprites. *Journal of Geophysical Research*, *109*, A04301. https://doi.org/10.1029/2003jA010064

Lu, G. (2006). Transient electric field at high altitudes due to lightning: Possible role of induction field in the formation of elves. *Journal of Geophysical Research*, *111*, D02103. https://doi.org/10.1029/2005JD005781

Lu, G., Cummer, S. A., Chen, A. B., Lyu, F., Li, D., Hsu, R. R., & Su, H.-T. (2017). Analysis of lightning strokes associated with sprites observed by ISUAL in the vicinity of North America. *Terrestrial, Atmospheric and Oceanic Sciences*, *28*(4), 583–595. https://doi.org/10.3319/TAO.2017.03.31.01

Lu, G., Cummer, S. A., Li, J., Zigoneanu, L., Lyons, W. A., Stanley, M. A., et al. (2013). Coordinated observations of sprites and in-cloud lightning flash structure. *Journal of Geophysical Research - D: Atmospheres*, *118*(12), 6607–6632. https://doi.org/10.1002/jgrd.50459

Lyons, W. A. (1996). Sprite observations above the U.S. High Plains in relation to their parent thunderstorm systems. *Journal of Geophysical Research: Atmospheres*, *101*(D23). 29641–29652. https://doi.org/10.1029/96JD01866

Marshall, R. A. (2012). An improved model of the lightning electromagnetic field interaction with the D-region ionosphere. *Journal of Geophysical Research*, *117*(A3), A03316. https://doi.org/10.1029/2011JA017408

Morrill, J. S., Bucsela, E. J., Pasko, V. P., Berg, S. L., Heavner, M. J., Moudry, D. R., et al. (1998). Time resolved N2 triplet state vibrational populations and emissions associated with red sprites. *Journal of Atmospheric and Solar-Terrestrial Physics*, *60*(7–9), 811–829. https://doi.org/10.1016/S1364-6826(98)00031-5

Nagano, I., Yagitani, S., Miyamura, K., & Makino, S. (2003). Full-wave analysis of elves created by lightning-generated electromagnetic pulses. *Journal of Atmospheric and Solar-Terrestrial Physics*, *65*, 615–625. https://doi.org/10.1016/S1364-6826(02)00324-3

Newsome, R. T., & Inan, U. S. (2010). Free-running ground-based photometric array imaging of transient luminous events. *Journal of Geophysical Research*, *115*(A7), A00E41. https://doi.org/10.1029/2009JA014834

Pasko, V. P., Inan, U. S., & Bell, T. F. (1997). Sprites as evidence of vertical gravity wave structures above mesoscale thunderstorms. *Geophysical Research Letters*, *24*(14), 1735–1738. https://doi.org/10.1029/97GL01607

Pasko, V. P., Inan, U. S., & Bell, T. F. (1998). Spatial structure of sprites. *Geophysical Research Letters*, *25*(12), 2123–2126. https://doi.org/10.1029/98GL01242

Pasko, V. P., Inan, U. S., & Bell, T. F. (1999). Mesospheric electric field transients due to tropospheric lightning discharges. *Geophysical Research Letters*, *26*(9), 1247–1250. https://doi.org/10.1029/1999GL900240

Pasko, V. P., Inan, U. S., Bell, T. F., & Taranenko, Y. N. (1997). Sprites produced by quasi-electrostatic heating and ionization in the lower ionosphere. *Journal of Geophysical Research*, *102*(A3), 4529–4561. https://doi.org/10.1029/96JA03528

Qin, J., Celestin, S., & Pasko, V. P. (2011). On the inception of streamers from sprite halo events produced by lightning discharges with positive and negative polarity. *Journal of Geophysical Research*, *116*, A06305. https://doi.org/10.1029/2010JA016366

Qin, J., Pasko, V. P., McHarg, M. G., & Stenbaek-Nielsen, H. C. (2014). Plasma irregularities in the D-region ionosphere in association with sprite streamer initiation. *Nature Communications*, *5*, 3740. https://doi.org/10.1007/s11430-018-9311-y

Ren, H., Tian, Y., Lu, G., Zhang, Y., Fan, Y., Jiang, R., et al. (2019). Examining the influence of current waveform on the lightning electromagnetic field at the altitude of halo formation. *Journal of Atmospheric and Solar-Terrestrial Physics*, *189*, 114–122. https://doi.org/10.1016/j.jastp.2019.04.010

Rowland, H. L. (1998). Theories and simulations of elves, sprites and blue jets. *Journal of Atmospheric and Solar-Terrestrial Physics*, *60*(7-9), 831–844. https://doi.org/10.1016/S1364-6826(98)00034-0

Sentman, D. D., Wescott, E. M., Osborne, D. L., Hampton, D. L., & Heavner, M. J. (1995). Preliminary results from the Sprites94 Aircraft Campaign: 1. Red sprites. *Geophysical Research Letters*, *22*(10), 1205–1208. https://doi.org/10.1029/95GL00583

Stanley, M., Krehbiel, P., Brook, M., Moore, C., Rison, W., & Abrahams, B. (1999). High speed video of initial sprite development. *Geophysical Research Letters*, *26*(20), 3201–3204. https://doi.org/10.1029/1999GL010673

Stenbaek-Nielsen, H. C., Kanmae, T., McHarg, M. G., & Haaland, R. (2013). High-speed observations of sprite streamers. *Surveys in Geophysics*, *34*(6), 769–795. https://doi.org/10.1007/s10712-013-9224-4

Taranenko, Y. N., Inan, U. S., & Bell, T. F. (1993). Interaction with the lower ionosphere of electromagnetic pulses from lightning: Heating, attachment, and ionization. *Geophysical Research Letters*, *20*(15), 1539–1542. https://doi.org/10.1029/93GL01696

Thomas, J. N., Holzworth, R. H., McCarthy, M. P., & Pinto, O., Jr. (2005). Predicting lightning-driven quasi-electrostatic fields at sprite altitudes using in situ measurements and a numerical model. *Geophysical Research Letters*, *32*, L10809. http://doi.org/10.1029/2005GL022693

Wescott, E. M., Stenbaek-Nielsen, H. C., Sentman, D. D., Heavner, M. J., Moudry, D. R., & Sabbas, F. T. S. (2001). Triangulation of sprites, associated halos and their possible relation to causative lightning and micrometeors. *Journal of Geophysical Research*, *106*(A6), 10467–10477. https://doi.org/10.1029/2000ja000182

Winckler, J. R. (1995). Further observations of cloud-ionosphere electrical discharges above thunderstorms. *Journal of Geophysical Research*, *100*(D7), 14335–14345. https://doi.org/10.1029/95JD00082

Yue, J., & Lyons, W. A. (2015). Structured elves: Modulation by convectively generated gravity waves. *Geophysical Research Letters*, *42*(4), 1004–1011. https://doi.org/10.1002/2014GL062612

Zhang, Q. L., Tian, Y., & Lu, G. P. (2014). Effects of the nonlinear atmosphere electric parameters at the high altitudes on the propagation of lightning return stroke electromagnetic field. *Acta Meteorologica Sinica*, *72*(4), 805–814. https://doi.org/10.11676/qxxb2014.045